Transverse Jet-Cavity Interactions with the Influence of an Impinging Shock

H. Zare-Behtash,* K. H. Lo, and K. Kontis

School of Engineering, University of Glasgow, Scotland G12 8QQ, UK

T. Ukai and S. Obayashi

Institute of Fluid Science, Tohoku University, Sendai, Miyagi, 980-8577, Japan

Abstract

For high-speed air breathing engines, fuel injection and subsequent mixing with air is paramount for combustion. The high freestream velocity poses a great challenge to efficient mixing both in macroscale and microscale. Utilising cavities downstream of fuel injection locations, as a means to hold the flow and stabilise the combustion, is one mechanism which has attracted much attention, requiring further research to study the unsteady flow features and interactions occurring within the cavity. In this study we combine the transverse jet injection upstream of a cavity with an impinging shock to see how this interaction influences the cavity flow, since impinging shocks have been shown to enhance mixing of transverse jets. Utilising qualitative and quantitative methods: schlieren, oilflow, PIV, and PSP the induced flowfield is analysed. The impinging shock lifts the shear layer over the cavity and combined with the instabilities generated by the transverse jet creates a highly complicated flowfield with numerous vertical structures. The interaction between the oblique shock and the jet leads to a relatively uniform velocity distribution within the cavity.

*Hossein.Zare-Behtash@glasgow.ac.uk

I. INTRODUCTION

The introduction of this paper is focused on two different flow phenomena, namely, transverse jets and cavities in supersonic flow. Although these two topics may seem disconnected at first, they are brought together through this research.

Transverse jet injection into supersonic/hypersonic flows has several engineering applications ranging from flow control and attitude control, by creating forces and moments, to fuel injection in scramjets and thrust vector control.[1–9] Such flows are extremely complicated and unsteady, making the numerical and experimental studies of such phenomena very difficult and challenging.

For the application in scramjet combustion, due to the millisecond residence times of the flow, efficient mixing is key.[10–12] Mai et al.[13] showed that by having an incident shock impinge close to the transverse jet injection location, an enhanced mixing level can be achieved with an increased residence time that would lead to a more efficient combustion. Similar findings were reported by Schetz et al.[14] regarding the increased mixing levels during shock-jet interactions and also the location of the impinging shock which results in the best mixing, that is, when the shock impinges immediately downstream of the jet. The enhancing combustion properties of impinging shocks is also documented by Huh and Driscol,[15] where the authors believe that it is the adverse pressure gradient caused by shock that is responsible for altering the recirculation zones and leading to flame stability.

According to Lazar et al.[16] cavities represent a fundamental fluid dynamic configuration, with applications ranging from supersonic aircraft weapon bays and the problems associated with aerodynamic drag and heating to high-speed combustion. Employing cavities inside scramjets is a mechanism to improve combustion by decelerating the breathing air from supersonic to subsonic speeds in order for combustion to occur. Supersonic flows over cavities lead to extremely unsteady flows, requiring detailed analysis and design consideration. As evident from the schlieren photograph of Figure 1, in all flows over a cavity a shear layer is present, which develops out of the boundary layer behind the leading edge of the cavity and is sustained by the velocity difference between the freestream and the flow inside the cavity. In supersonic flows an oblique shock forms at the leading edge of the cavity due to the separation of the boundary layer and an expansion or compression wave is similarly seen at the trailing edge. As the shear layer separates from the leading edge of the cavity, it starts

to roll up into large-scale vortical structures due to the KelvinHelmholtz instability. When these structures impinge on the trailing edge of the cavity, acoustic waves are generated. These waves propagate to the leading edge within the cavity, because the free-stream flow is supersonic, to further excite the shear layer.[17]

Gruber et al.[18] looked at how changes in the aft wall of an open cavity can lead to changes in the shear layer and hence the drag and residence time within the cavity. Sakamoto et al.[19] revealed the complex three-dimensional nature of two-dimensional cavity flows, and the oscillatory nature of the leading edge cavity shock. When introducing an impinging shock over the cavity, they found that the shear layer angle, separation lines, and the features of the bow shock at the rear corner of the cavity depend strongly on the impinging shock location. Ukai et al.[20] showed that if an injector is positioned close to the cavity leading edge, not only is the mixing enhanced within the cavity, but a stable mixing can be achieved independent on the jet-to-freestream momentum flux ratio.

According to Ben-Yakar and Hanson[21] flame holding is achieved by: 1) organisation of a recirculation area where the fuel and air can be mixed partially at low velocities, and 2) interaction of a shock wave with partially or fully mixed fuel and oxidizer; both of these methods can be found in the present study. It is therefore the goal of this study to examine the flow physics when combining an impinging shock wave with a transverse jet located upstream of a cavity. It is believed that combining the merits of enhanced jet mixing due to an impinging shock together with placing a cavity downstream, higher levels of mixing and flow stability can be achieved. It is believed that the results will not only shed light on the fundamental flow characteristics but also help in the development and verification of advanced turbulence modelling tools.

II. EXPERIMENTAL SETUP

A. Wind tunnel and model

The wind tunnel, identical to that used by Ukai et al.,[20] is an intermittent indraft tunnel with test section dimensions of 150×215×485mm (width×height×length). Desiccant particles are present at the tunnel inlet to absorb the moisture in the air, a heater is used to dry the desiccants and relieve them of any moisture content. For a Mach number of 1.9, the

tunnel has a stable run time of approximately 5 seconds and a Mach number variation of ± 0.01 for different runs. The Reynolds number for the current experiments is 8.4×10^6/m. Although previous studies examining scramjet flow physics have covered higher Mach numbers and Reynolds numbers in the 10^6 regime,[22] the flow inside the combustion chamber of a scramjet would be travelling at a much lower Mach number due to the various compression waves encountered upstream.[23]

As shown in Figure 2, a shock generator with a wedge angle of 10 degrees is mounted on the top wall of the test section to generate an oblique shock wave. The location of the shock generator can be varied in the streamwise sense. Two locations are chosen, Case 1 immediately downstream of the jet location, and Case 2 where the shock wave impinges 7.5mm downstream of the cavity leading edge.

A rectangular open cavity, 100mm in length (L) and 20mm deep (D), was designed into the bottom wall of the test section. An axisymmetric conical jet hole with an orifice diameter of di=2.2mm was placed 10mm ($0.1L$) upstream of the cavity along the centreline, with air as the jet medium. A jet to freestream momentum flux ratio, measure of the jet penetration into the freestream, of 5.3 was chosen, identical to the work of Ukai et al.[20,24] which is defined in Eq. (1),

$$J = \frac{\gamma_{jet} p_{jet} M_{jet}^2}{\gamma_o p_o M_o^2} \tag{1}$$

where γ denotes specific heat ratio, p pressure, M Mach number, and the subscripts "o" and "jet" refer to the freestream and jet conditions, respectively.[12]

B. Measurement Techniques

A standard Z-type schlieren system was utilised, identical to that used by Zare-Behtash et al.[25,26] The light source was a 450W continuous Xenon lamp and a Photron SA-1 high-speed camera was used to capture images at a frame rate of 10kfps with an exposure time of 1μs.

Oil flow visualisation is a simple and effective method for visualising surface flow patterns.[27] Here, a mixture of fluorescent powder, paraffin, oleic acid, and silicon oil was used to map the flow. Before each run, the oil is deposited inside the cavity near the rear wall and illuminated with a pair of UV LED panels, 390nm wavelength, from both sides of

the test section. Images are acquired using a Canon SLR camera, model EOS-450D, with a 12M pixel resolution. The recipe was optimised through trial and error to ensures that the oil does not dry too quickly, allowing sufficient time for the flow to establish, but at the same time it is not too viscous to obstruct the flow.

For particle image velocimetry, a Litron Nano L series, ND:YAG Q-switched laser, 532nm wavelength, 4ns pulse duration, 200mJ/pulse and 15Hz repetition rate, was used for illumination along the centreline of the cavity. The time averaged flow field measurements consist of 60 image pairs captured with a Δt of 0.9μs. The Δt was recommended by the software, which is dependent on the field of view and the freestream velocity. A laser arm was used to deliver the laser to the test section. To create tracer particles a TSI six-jet atomiser model 9307-6 was used. The seeder is capable of creating particles with a diameter of approximately 1μm.[28] A LaVision Imager ProX CCD camera with 1600×1200 pixel resolution was used for image capture at 14 bit digitisation. The recorded image pairs are initially divided into 32×32 pixel interrogation windows and then processed with a cross correlation algorithm using the DaVis 7.2 software, the interrogation windows are then refined to 16×16 pixel squares.

The total uncertainty of the PIV measurements, taking into account the error arising during the cross-correlation process,[29] the accuracy of the seeder particles to follow the flow streamline,[30] and also the uncertainty in velocity measurement using PIV,[31] is calculated at ± 6.5%.

The Pressure sensitive paint (PSP) technique was also utilised. The description of this technique along with its merits over conventional pressure measurement techniques are well documented in the literature.[32–37] The in-house developed PSP technology used in the present study has been successfully applied in a variety of flow conditions and has been found in all cases to provide accurate pressure measurements when compared to conventional pressure transducers.[38–44] The PSP setup consists of a LaVision Image Intense 12-bit CCD camera with a 590nm long-pass filter mounted on the lens, and UV LEDs with peak wavelength of 390nm were used for image acquisition. Ruthenium is used as the luminophore molecules in the current recipe. Multiple images were collected and then summed to improve the signal to noise ratio of the collected data. The PSP was sprayed over the cavity floor over a matte white coat, and the camera was mounted on the top wall looking down onto the cavity.

A dark image is subtracted from the wind-on (with flow) and wind-off (no flow) images to account for variations in the dark current signal of the camera. An in-house developed Matlab code is used for image processing. The code also carries out an image registration to eliminate any errors due to model movement during the experiments. An a-priori calibration was applied to the data, since in-situ calibration was not possible in the current setup. Temperature errors are usually associated with PSP measurements. Due to the low speed flow near the cavity floor, the recovery temperature approaches the flow stagnation temperature, and the fact that the model is made from aluminium, that has a high thermal conductivity, all contribute to an isothermal boundary condition.[45]

Pressure tappings were also placed along the cavity floor. However due to the tunnel design, long tubes were required to connect these to the transducers. The length of these tubes combined with the relatively short flow duration meant that the pressure data were unreliable.

III. RESULTS AND DISCUSSION

Instantaneous schlieren photographs of the flow are presented in Figure 3. From these images, the boundary layer thickness upstream of the cavity is calculated as 8.1mm. From the separation of the boundary layer at the leading edge of the cavity, a shear layer is formed. Downstream, the shear layer becomes less visible due to its unsteady nature. At the rear corner of the cavity a bow shock is formed due to the impingement of supersonic flow at this location. Figures 3(a) and (b) correspond to Case 1, shock immediately downstream of the jet, whereas Figures 3(c) and (d) show Case 2 with the impinging shock downstream of the cavity leading edge. At the front corner of the cavity typically an oblique shock wave is induced by the shear layer, however in the present study the interaction between the impinging shock in Figure3(a) leads to a different flow structure. When an incident shock impinges on a boundary layer it creates a reflected shock, whilst at the same time lifting the boundary layer and creating a virtual bump. Depending on the strength of this interaction, a region of reversed flow is some times created within this virtual bump. Due to the strong interaction of the impinging shock and boundary layer a separation shock is formed immediately upstream of the impinging shock. Traces of a weak recompression shock are also visible in this picture.

In Figure 3(c), the impinging shock occurs over the cavity and on the shear layer, however the interaction results in a similar interaction as with the boundary layer,[46] namely the lifting of the shear layer. Because the shear layer is lifted, the boundary layer separation at the leading corner of the cavity is moved further upstream, i.e., separation occurs earlier, and so the oblique separation shock from the cavity corner moves upstream. This behaviour is evident when comparing the case with the impinging shock to the undisturbed cavity case shown in Figure 4. When the jet is switched on in Figures 3(b) and (d), the presence of the jet moves the separation shock further upstream for both shock impingement locations.

Surface oil flow visualisations along with the streamlines are shown in Figure 5. The model centreline marked by the dashed line also crosses the centreline of the upstream jet. Wall effects occurring close to the cavity sides are evident. With no jets, the cavity floor is dominated by a strong flow originating from the rear face and terminating in two counter rotating vortices in Figures 5(a) and (c). When the jet is switch on, depicted in Figures 5(b) and (d), the presence of the jet leads to a relatively lower pressure along the centreline of the cavity floor (corroborated by the PSP measurements in Figure 9) compared to the sides. This gradient in pressure causes the air from the cavity sides to converge along the centreline and push the two large vortices closer together.

While the individual PIV measurements are likely to be accurate, the uncertainty associated with the possible lack of sufficient vector fields, to ensure statistical convergence, needs to be first addressed. As indicated in Figure 6, six random locations in the field of view were selected as samples and their stream-wise velocity component compared to. As evident in Figure 6(a), the obtained velocities tend to converge for the current ensembles with 60 vector fields. The standard error of the ensembles (standard deviation/square root of the population size), in Figure 6(b), decreases substantially as the number of vector fields increases. The sample points P5 and P6 exhibit higher error since they are located into the shear layer and cavity region, respectively, hence being influenced by the high instability of the flow.

The time averaged absolute flowfield velocity and streamlines for both cases is presented in Figure 7. Corroborating the schlieren images the impinging shock in Figures 7(a) and (c), with the jet off, raises the boundary and shear layer. This behaviour is further confirmed by examining Figure 8 which shows the flow over the same cavity with identical flow properties (the scales are slightly different). The boundary layer upstream of the cavity leading edge

is flat and parallel to the wall for the case with no shock impingement. Comparing this to the PIV results of Figures 7(a) and (c), in these figures the boundary layer is clearly lifted. For Case 1 in Figure 7(a), the shear layer downstream of the interaction remains horizontal and propagates downstream. For Case 2 however, in Figure 7(c), the raising of the shear layer is accompanied by a subsequent dip in its profile.

When the jet is switched on, see Figures 7(b) and (d), the flowfield characteristics are considerably different. Based on the work of Gruber et al.[4,47] and Ukai et al.,[24] the interaction between the jet and incoming flow leads to the creation of new vortical structures, leading to the amplification of the turbulence with the boundary layer and shear layer. The new structures created by the transverse jet are a combination of the influence of the jet bow shock and recirculation regions before and after the jet injection location. The presence of the jet not only thickens the shear layer but also lifts it higher. With the jet on, the flow structure inside the cavity is also different between Case 1 and Case 2. In Figure 7(b), the presence of a large vortex towards the aft wall of the cavity is evident. For Case 2, however, this vortex appears to be much smaller and closer to the aft wall. The streamlines of Figure 7(d) indicate that there is a greater transfer of mass and momentum between the cavity and the freestream in Case 2.

The pressure along the cavity centreline, obtained from PSP data, is provided in Figure 9 for the two cases with and without the jet. The uncertainty in the PSP measurements is $\pm 4.4\%$.[48] For both shock locations, the pressure is higher when the jet is switched on. The higher measured pressure, along the model centreline, indicates that with the introduction of the jet the flow speed along the cavity floor is reduced. This is consistent with the PIV data of Figures 7(b) and (d), where the shear layer thickness over the cavity increases with the introduction of the jet changing the vortex structures inside the cavity. A distinct difference between the two shock impingement cases is the pressure rise (looking from X = 220 pixels towards the cavity fore-wall) labelled in Figure 9(a). The location of this pressure rise corresponds to the recirculation region near the fore wall of the cavity. Since the rise in pressure appears for the jet off and on cases, it means that it is as a result of the shock interaction and its impingement location. It appears that the impinging shock reduces the strength of the vortex near the fore wall, leading to a lower induced velocity and therefore higher static pressure. This, however, needs to be substantiated by comparing the pressure measurements from an undisturbed cavity. High resolution PIV measurements focusing on

this small region are necessary to extract the exact flow structures.

Because the two shock impingement cases with no jet exhibit a similar time averaged velocity profile, taking Case 1 where the shock impinges immediately downstream of the jet, the root mean square of the Vx (longitudinal) and Vy (transverse) components of velocity profile are presented in Figure 10. It is clear from this data that for the present open cavity case, the longitudinal oscillations, running along the cavity, are the dominant structures responsible for the mass and momentum transfer in and out of the cavity. This behaviour was also observed for Case 2 with the jet off, and with the jet on for both cases. For small cavities (L/D $<$ 2-3) transverse oscillation dominate the cavity unsteadiness whereas for larger aspect ratio cavities longitudinal oscillation are the dominant mechanism. The impingement of the shear layer at the aft wall introduces freestream flow into the cavity. This impingement creates acoustic or compression waves inside the cavity.[21] The propagation of these compression wave inside the cavity result in the high rms value of the V_x component.

The turbulence Reynolds stress, Re_{xy} is an important dynamic quantity affecting the mean flow since it is responsible for a major part of the momentum transfer due to turbulent fluctuations. The Reynolds stress is not only an indicator of the r.m.s. velocities but also related to vorticity which is has strong influence on mixing, making it a suitable parameter to analyse. The calculated Reynolds stresses are provided in Figure 11. The highest concentration of Re_{xy} occurs near the aft wall of the cavity since this is where the dominant vortex structure inside the cavity exists. With the introduction of the jet in Figures 11(b) and (d), Case 1 shows a greater area of the cavity covered by turbulent structures originating from the transverse jet.

Profiles of the Reynolds stress taken at three different locations along the cavity floor: $0.2L$, $0.5L$, and $0.8L$ (L being the length of the cavity) are plotted in Figure 12 for each subfigure of Figure 11. The profiles corresponding to Case 2, Figures 12(c) and (d), show higher magnitudes of Re_{xy} near the aft wall compared to Case 1. The profiles of Case 1 indicate the presence of smaller structures and greater in number, this is induced from the greater number of fluctuations in Re_{xy} as we move from $Y = 0mm$ at the cavity floor to $Y = 50mm$ in the shear layer. To clarify this behaviour, Figure 13 shows the Re_{xy} profiles for the two shock impingement locations with jet on at x = 0.5L. The greater number of fluctuations is deduced from the higher number of peaks in the profile for Case 1.

Examining the Reynolds stress near the leading edge wall of the cavity in Figure 14, it

is evident that for Case 1, where the shock impinges near the jet location, the region where the Re_{xy} has a lower magnitude near the fore-wall is smaller in size compared to Case 2. In terms of mixing, this implies that in Case 1 a larger area of mixing is present inside the cavity, leading to an enhanced overall mixing.

IV. CONCLUSIONS

The current investigation analysed experimentally the flow characteristics of a transverse jet injection upstream of an open cavity with the influence of an impinging shock. The results reveal that the location of the impinging shock influences the cavity flow. The interaction between the vortical structures created by the transverse jet and the impinging shock changes the geometry of the shear layer over the cavity. The streamlines showed that when the shock impinges near the cavity leading edge, the lifting of the shear layer encourages a greater momentum transfer into the freestream near the cavity aft wall. The shock impingement location also influences the vortex structure inside the cavity. When the shock wave impinges close to the jet, the strength of the vortex near the cavity fore-wall is reduced leading to a lower induced velocity near the bottom wall.

Analysis of the Reynolds stress inside the cavity reveal that when the jet is introduced and the shock impinges close to the jet, a greater area of the cavity is covered by turbulent structures originating from the transverse jet. The Reynolds stress also shows an enhancement in mixing occurring the cavity fore-wall for the aforementioned case, deduced by the larger area of high of Reynolds stress magnitude.

We can conclude from the findings presented here that the case where the shock impinges close to the jet leads to the creation of a greater number of smaller turbulent structures compared to when the shock impinges on the cavity corner. Given the 3D nature of using a single jet to force the cavity flow, high resolution PIV experiments focusing on specific areas of the cavity a recommended. These will provide a more comprehensive insight into the flow interactions. What remains to be seen is how the variation in turbulence and therefore mixing resulted from the shock interaction influences parameters such as residence time, burn percentage, thrust production and also the generation of noise inside a scramjet.

It is recommended that the number of vector fields collected for the PIV analysis be increased so that a higher level of convergence can be achieved, thereby increasing the

accuracy of the time-averaged results.

Acknowledgments

The authors are grateful to the technical and administrative staff at the university, and to the EPSRC engineering equipment loan pool, especially Mr. Adrian Walker, for the loan of the Photron camera. This paper is dedicated to the hard work and talents of Mr. Lee Paul who manufactured the models and has recently left the department.

[1] Ferri, A., Nucci, L.M., "Preliminary investigation of a new type of supersonic inlet," *NACA-TN-2286* (1951).

[2] Sullins, G.A., "Demonstration of mode transition in a scramjet combustor," *Journal of Propulsion and Power* **9**, 515–520, (1993).

[3] Ali, M., Fujiwara, T., Leblanc, J.E., "Influence of main flow inlet configuration on mixing and flameholding in transverse injection into supersonic airstream," *International Journal of Engineering Science* **38**, 1161–1181, (2000).

[4] Gruber, M.R., Nejad, A.S., Chen, T.H., Dutton, J.C., "Transverse injection from circular and elliptic nozzles into a supersonic crossflow," *Journal of Propulsion and Power* **16**, 449–457, (2000).

[5] Kontis, K., "Jet control effectiveness studies on a flat-plate body at hypersonic speeds," *Transactions of the Japan Society for Aeronautical and Space Sciences* **47**, 131–137, (2004).

[6] Lee, S.H., "Characteristics of dual transverse injection in scramjet combustor, Part 1: Mixing," *Journal of Propulsion and Power* **22**, 1012–1019, (2006).

[7] Lee, S.H., "Characteristics of dual transverse injection in scramjet combustor, Part 2: Combustion," *Journal of Propulsion and Power* **22**, 1020–1026, (2006).

[8] Erdem, E., Kontis, K., "Numerical and experimental investigation of transverse injection flows," *Shock Waves* **20**, 103–118, (2010).

[9] Cecere, D., Ingenito, A., Giacomazzi, E., Romagnosi, L., Bruno, C., "Hydrogen/air supersonic combustion for future hypersonic vehicles," *International Journal of Hydrogen Energy* **36**, 11969–11984, (2011).

[10] Tomioka, S., Jacobsen, L.S., Schetz, J.A., "Sonic injection from diamond-shaped orifices into a supersonic crossflow," *Journal of Propulsion and Power* **19**, 104–114, (2003).

[11] Burtschell, Y., Zeitoun, D.E., "Numerical investigation of H2 injection in Mach 5 air flow with a strong shock/boundary layer interaction," *Shock Waves* **13**, 465–472, (2004).

[12] Huang, W., Liu, W.D., Li, S.B., Xia, Z.X., Liu, J., Wang, Z.G., "Influences of the turbulence model and the slot width on the transverse slot injection flow field in supersonic flows," *Acta Astronautica* **73**, 1–9, (2001).

[13] Mai, T., Sakimitsu, Y., Nakamura, H., Ogami, Y., Kudo, T., Kobayashi, H., "Effect of the

incident shock wave interacting with transversal jet flow on the mixing and combustion," *Proceedings of the Combustion Institute* **33**, 2335–2342, (2011).

[14] Schetz, J.A., Maddalena, L., Burger, S.K., "Molecular weight and shock-wave effects on transverse injection in supersonic flow," *Journal of Propulsion and Power* **26**, 1102–1113, (2010).

[15] Huh, H., Driscoll, J.F., "Shock-wave-enhancement of the mixing and stability limits of supersonic hydrogen-air jet flames," *26th Symposium (International) on Combustion/The Combustion Institute*, 2933–2939, (1996).

[16] Lazar, E., Elliot, G., Glumac, N., "Control of the shear layer above a supersonic cavity using energy deposition," *AIAA Journal* **46**, 2987–2997, (2008).

[17] Zhuang, N., Alvi, F.S., Alkislar, M.B., Shih, C., "Supersonic cavity flows and their control," *AIAA Journal* **44**, 2118–2128, (2006).

[18] Gruber, M.R., Baurle, R.A., Mathur, T., Hsu, K.-Y., "Fundamental studies of cavity-based flameholder concepts for supersonic combustors," *Journal of Propulsion and Power* **17**, 146–153, (2001).

[19] Sakamoto, K., Matsunaga, K., Fujii, K., Tamura, Y., "Experimental investigation of supersonic internal cavity flows," *26th AIAA Fluid Dynamics Conference* AIAA-95-2213, (1995).

[20] Ukai, T., Obayashi, S., Zare-Behtash, H., Erdem, E., Lo, K.H., Kontis, K., "Effectiveness of jet location on mixing characteristics inside a cavity in supersonic flow," *Experimental Thermal and Fluid Science* (2013), **52**, 59–67, (2014).

[21] Ben-Yakar, A., Hanson, R.K., "Cavity flame-holders for ignition and flame stabilization in scramjets: An overview," *Journal of Propulsion and Power* **17**, 869–877, (2001).

[22] Holland, S.D., "Reynolds number and cowl position effects for a generic sidewall compression scramjet inlet at Mach 10 - A computational and experimental investigation," *17th Aerospace Ground Testing Conference*, Nashville, AIAA-92-4026, (1992).

[23] Che Idris, A., Saad, M.R., Zare-Behtash, H., Kontis, K., "Luminescent measurement systems for the investigation of a scramjet inlet-isolator," *Sensors* **14**, 6606–6632, (2014).

[24] Ukai, T., Zare-Behtash, H., Lo, K.H., Kontis, K., Obayashi, S., "Effects of dual jets distance on mixing characteristics and flow path within a cavity in supersonic crossflow," *International Journal of Heat and Fluid Flow* (2014), **In Press**.

[25] Zare-Behtash, H., Kontis, K., Gongora-Orozco, N., Takayama, K., "Compressible vortex loops: Effect of nozzle geometry," *International Journal of Heat and Fluid Flow* **30**, 561–576, (2009).

[26] Zare-Behtash, H., Gongora-Orozco, N., Kontis, K.,"Effect of primary jet geometry on ejector performance: A cold-flow investigation," *International Journal of Heat and Fluid Flow* **32**, 596–607, (2011).

[27] Lada, C., Kontis, K.,"Experimental studies on transitional and closed cavity configurations including flow control," *Journal of Aircraft* **47**, 723–730, (2010).

[28] Zare-Behtash, H., Kontis, K., Gongora-Orozco, N., Takayama, K., "Shock wave-induced vortex loops emanating from nozzles with singular corners," *Experiments in Fluids* **49**, 1005–1019, (2010).

[29] Lusl, W.T., "Control of Supersonic Cavity Flow by Leading Edge Blowing," *MPhill*, University of Florida, USA, (2011).

[30] Samimy, M., Lele, S.K., "Motion of particles with inertia in a compressible free shear layer," *Physics of Fluids* **3**, 1915–1923, (1991).

[31] Grant, I., Owens, E.H., "Confidence Interval Estimates in PIV Measurements of Turbulent Flows," *Applied Optics* **29**, 1400–1402, (1990).

[32] Carroll, B.F., Abbitt, J.D., Lukas, E.W., Morris, M.J., "Step response of pressure-sensitive paints," *AIAA Journal* **34**, pp. 521–526, 1996.

[33] Moshasrov, V., Radchenko, V., Fonov, S., "Luminescent Pressure Sensors in Aerodynamic Experiments," *Central Aerodynamic Institute (TsAGI)*, 1998.

[34] Bell, J.H., Schairer, E.T., Hand, L.A., Mehta, R.D., "Surface pressure measurements using luminescent coatings," *Annual Review of Fluid Mechanics* **33**, pp. 155–206, 2001.

[35] Kontis, K., Lada, C., Zare-Behtash, H., "Effect of dimples on glancing shock wave turbulent boundary layer interactions," *Shock Waves* **17**, pp. 323–335, 2008.

[36] Gregory, J.W., Asai, K., Kameda, M., Liu, T., Sullivan, J.P., "A review of pressure-sensitive paint for high-speed and unsteady aerodynamics," *Proceedings of the Institution of Mechanical Engineers, Part G: Journal of Aerospace Engineering* **222**, pp. 249–290, 2008.

[37] Yang, L., Zare-Behtash, H., Erdem, E., Kontis, K., "Application of AA-PSP to hypersonic flows: The double ramp model," *Sensors and Actuators B: Chemical* **161**, 100–107, (2012).

[38] Kontis, K., "A review of some current research on pressure sensitive paint and thermographic phosphor techniques," *The Aeronautical Journal* **111**, 495–508, (2007).

[39] Zare-Behtash, H., Gongora-Orozco, N., Kontis, K., "PSP visualization studies on a convergent nozzle with an ejector system," *Journal of Visualization* **12**, 157–163, (2009).

[40] Quinn, M.K., Yang, L., Kontis, K., "Pressure-sensitive paint: Effect of substrate," *Sensors* **11**, 11649–11663, (2011).

[41] Yang, L., Erdem, E., Zare-Behtash, H., Kontis, K., Saravanan, S., "Pressure-sensitive paint on a truncated cone in hypersonic flow at incidences," *International Journal of Heat and Fluid Flow* **37**, 9–21, (2012).

[42] Yang, L., Zare-Behtash, H., Erdem, E., Kontis, K., "Investigation of the double ramp in hypersonic flow using luminescent measurement systems," *Experimental Thermal and Fluid Science* **40**, 50–56, (2012).

[43] Quinn, M.K., Gongora-Orozco, N., Kontis, K., Ireland, P., "Application of pressure-sensitive paint to low-speed flow around a U-bend of strong curvature," *Experimental Thermal and Fluid Science* **48**, 58–66, (2013).

[44] Quinn, M.K., Kontis, K., "Pressure-sensitive paint measurements of transient shock phenomena," *Sensors* **13**, 4404–4427, (2013).

[45] Bjorge, S.T., Reeder, M.F., Subramanian, C. Crafton, J., Fonov, S., "Flow around an object projected from a cavity into a supersonic freestream," *AIAA Journal* **43**, 1465–1475, (2005).

[46] Babinksy, H., Harvey, J.K., "Shock wave-boundary layer interactions," *Cambridge University Press* 2011.

[47] Gruber, M.R., Baurle, R.A., Mathur, T., Hsu, K.-Y., "Mixing and penetration studies of sonic jets in a Mach 2 freestream," *Journal of Propulsion and Power* **11**, 315–323, (1995).

[48] Zare-Behtash, H., Gongora-Orozco, N., Kontis, K., Holder, S., "Application of novel pressure-sensitive paint formulations for the surface flow mapping of high-speed jets," *Experimental Thermal and Fluid Science* **33**, 852–864, (2009).

List of Figures

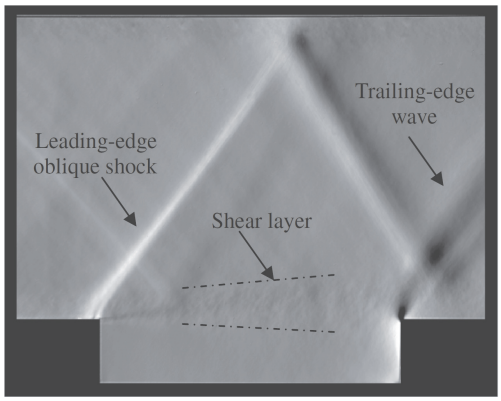

FIG. 1: Schlieren image of a typical supersonic flow over cavity.[16]

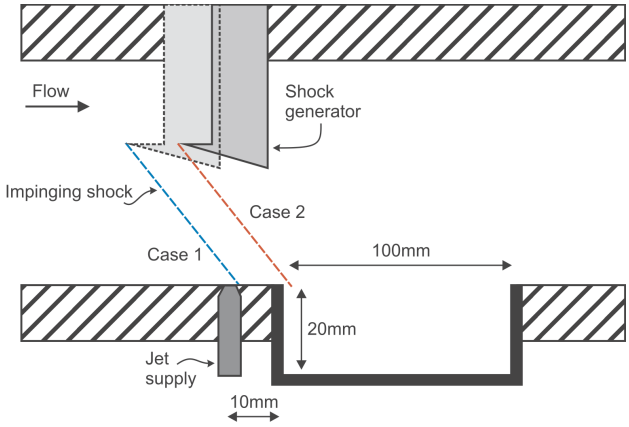

FIG. 2: Model arrangement and test cases for shock impingement.

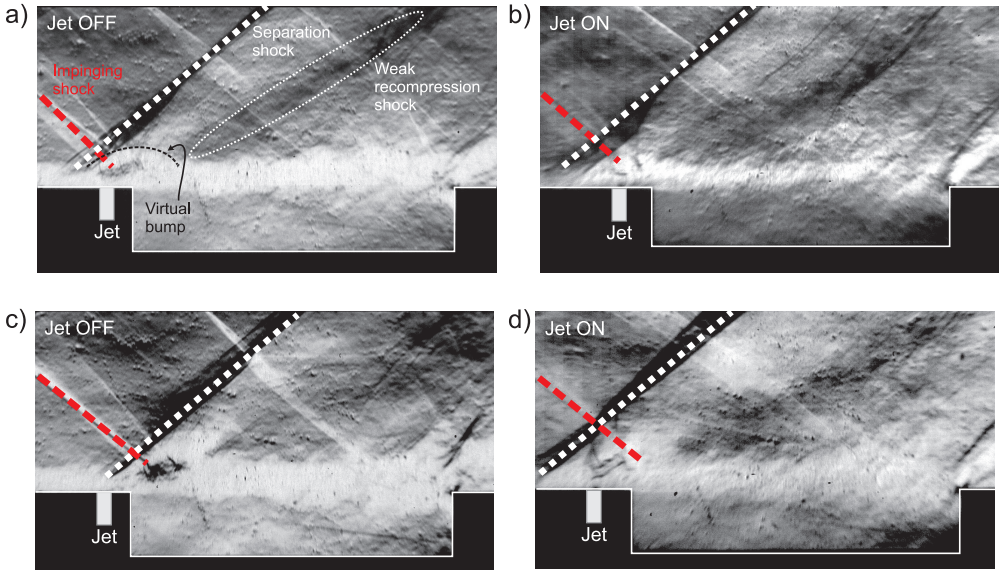

FIG. 3: Instantaneous schlieren images: (a) & (b) Case 1, (c) & (d) Case 2.

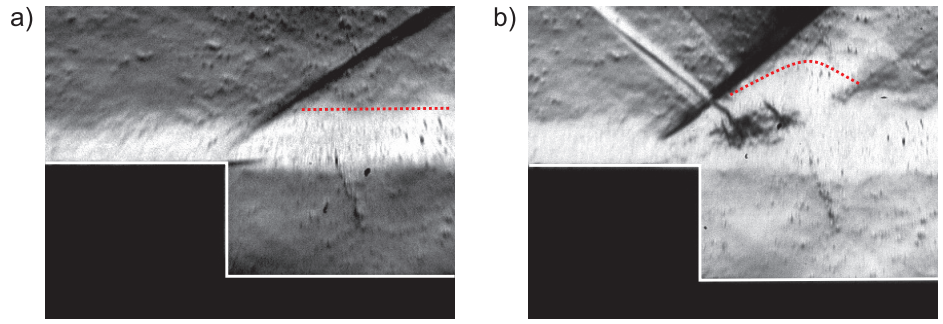

FIG. 4: Instantaneous schlieren images: (a) baseline,[24] (b) Case 2 corresponding to Figure 3(c).

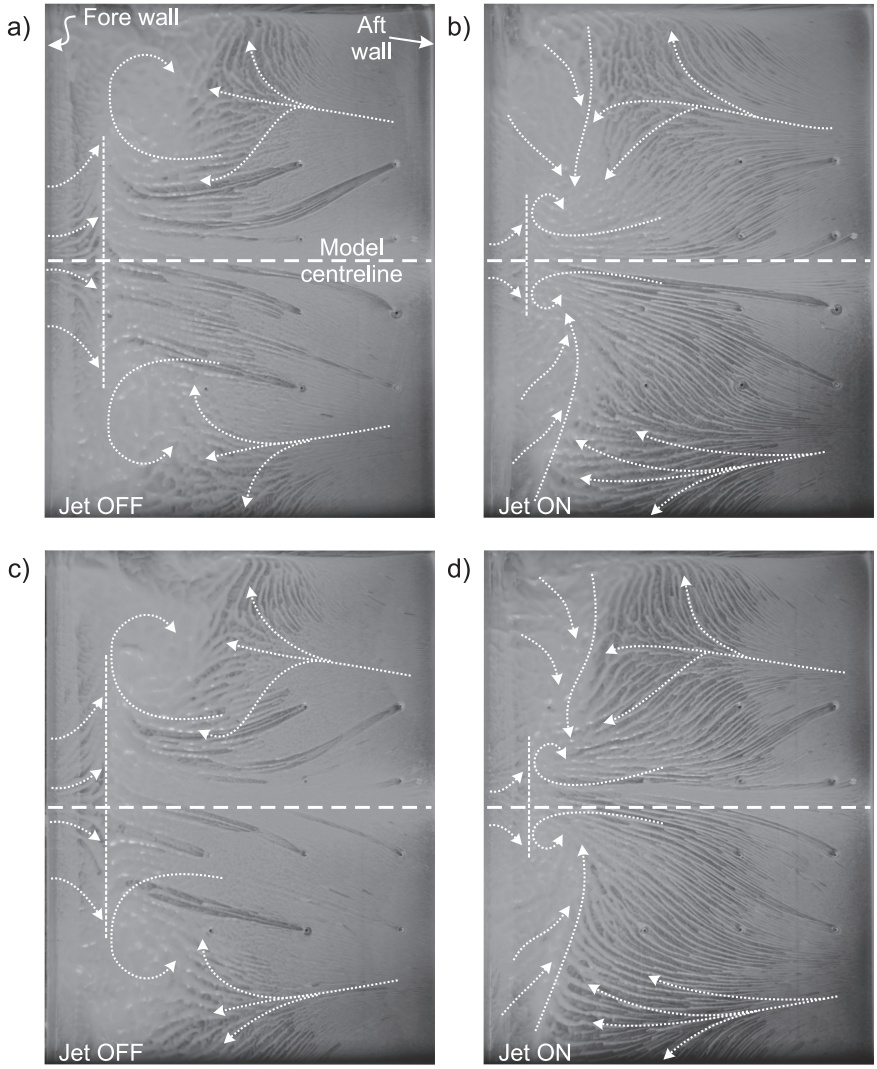

FIG. 5: Oil flow pattern along cavity floor: (a) & (b) Case 1, (c) & (d) Case 2.

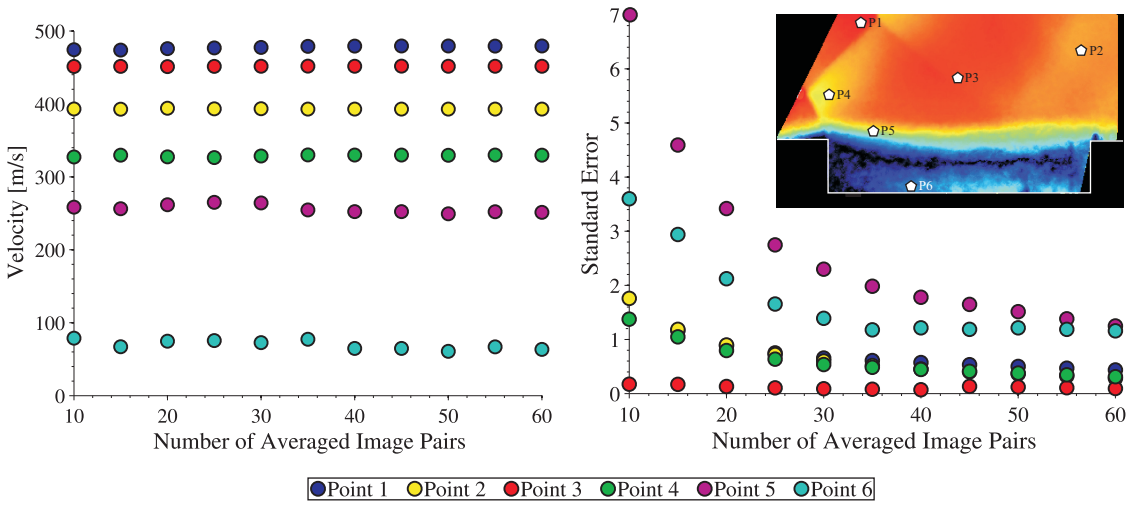

FIG. 6: PIV statistical analysis for increasing number of vector fields: (a) Convergence of velocity, (b) Standard error.

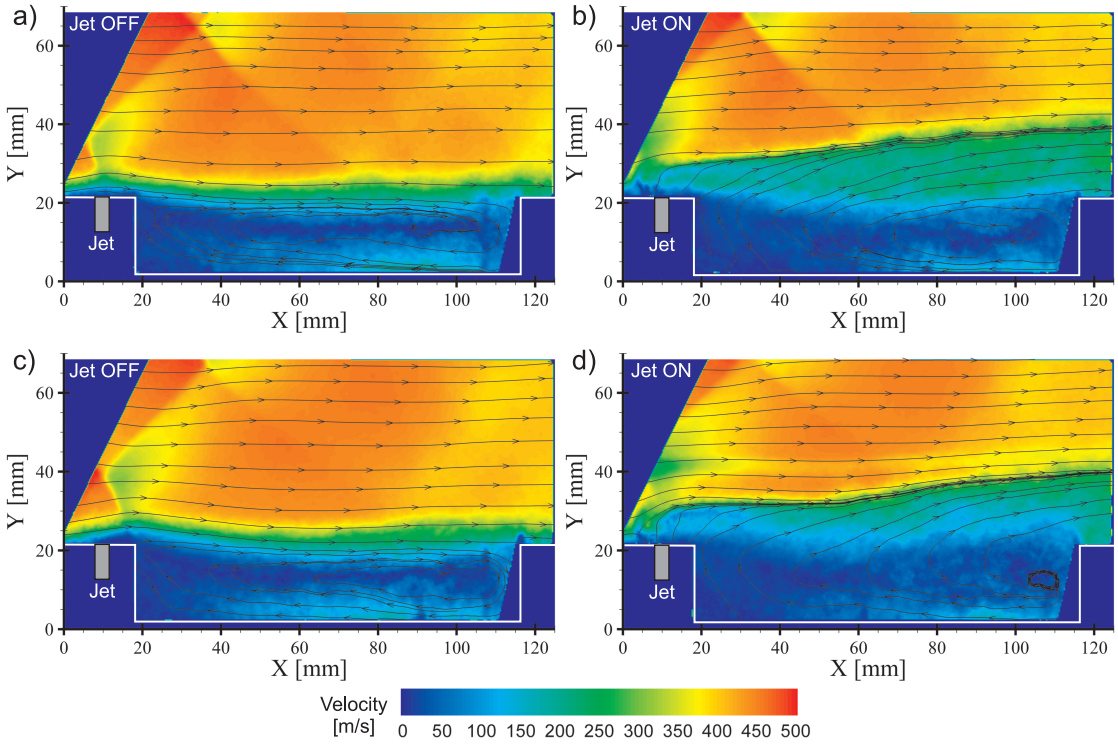

FIG. 7: Time average absolute velocity: (a) & (b) Case 1, (c) & (d) Case 2.

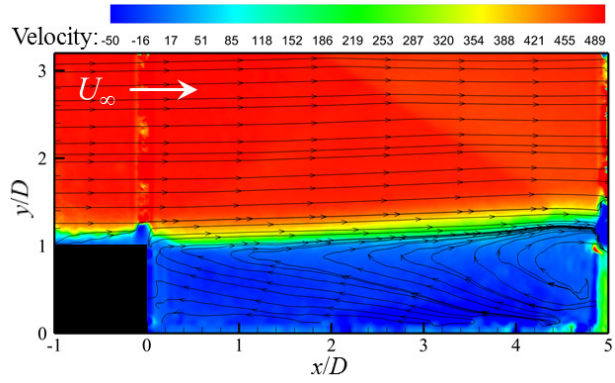

FIG. 8: Time average absolute velocity for the no-shock case taken from Ukai et al.[20]

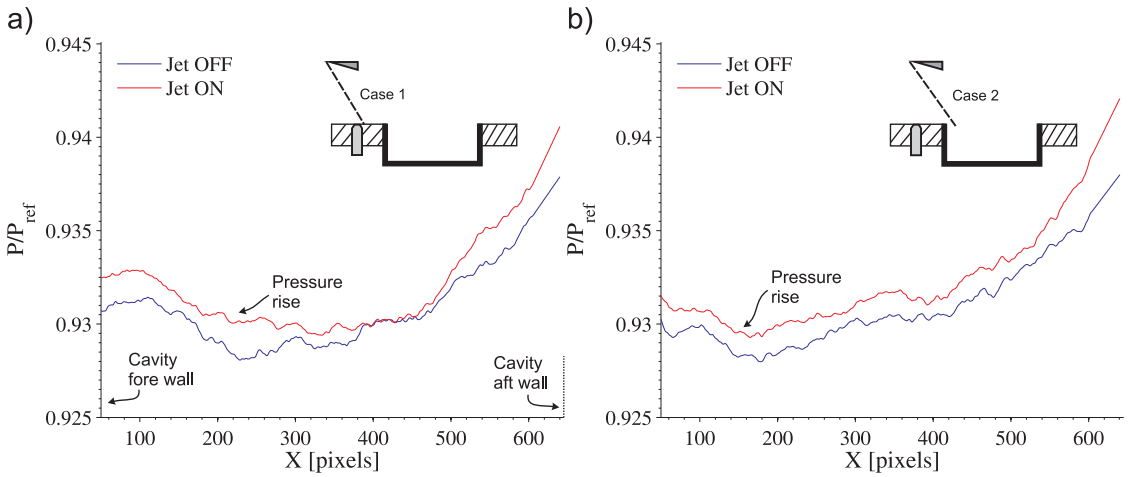

FIG. 9: PSP pressure profile along the centreline of the cavity, (a) Case 1, (b) Case 2.

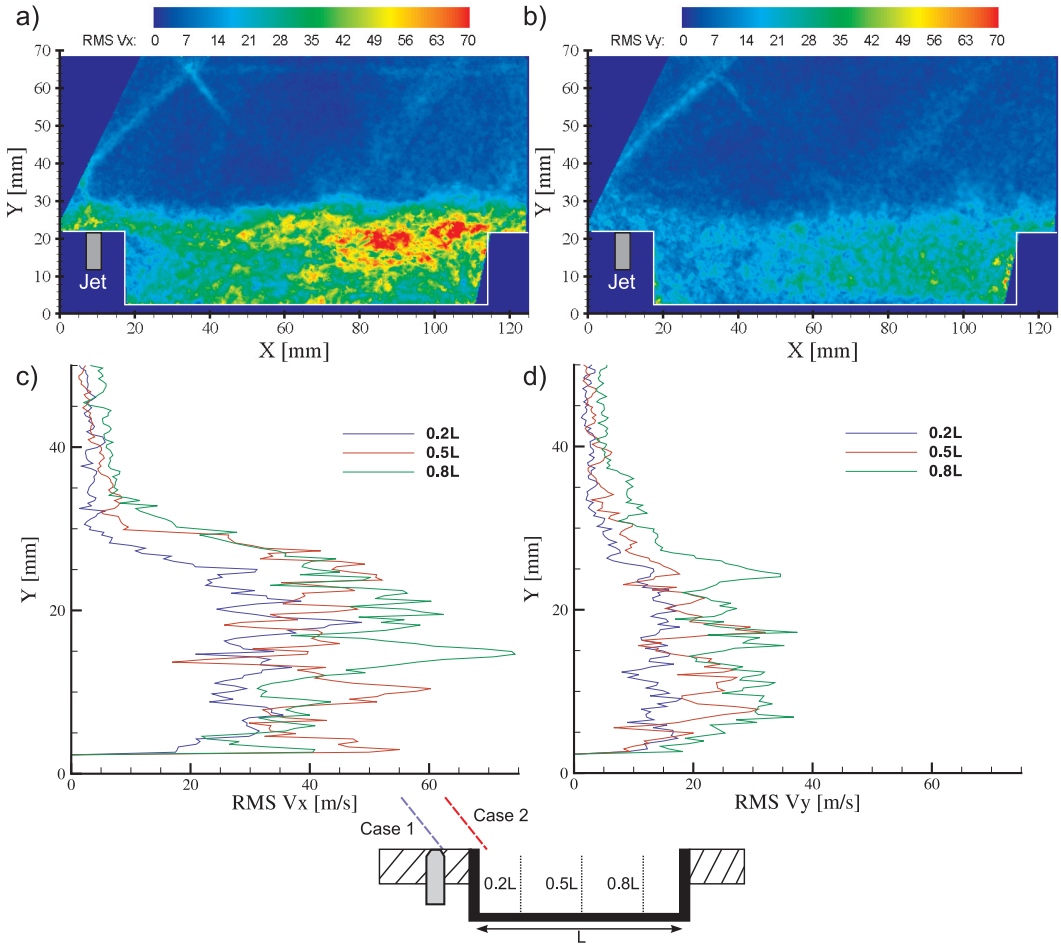

FIG. 10: Root mean square profiles of: (a) & (c) Vx and (b) & (d) Vy corresponding to Figure 7(a).

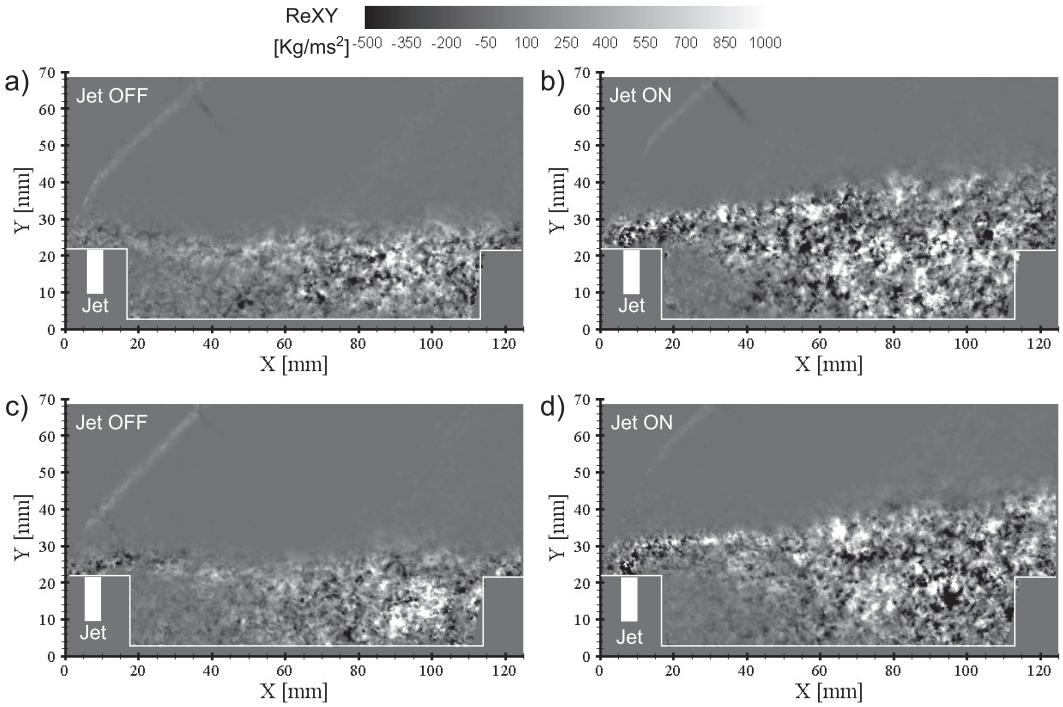

FIG. 11: Reynolds stress: (a) & (b) Case 1, (c) & (d) Case 2.

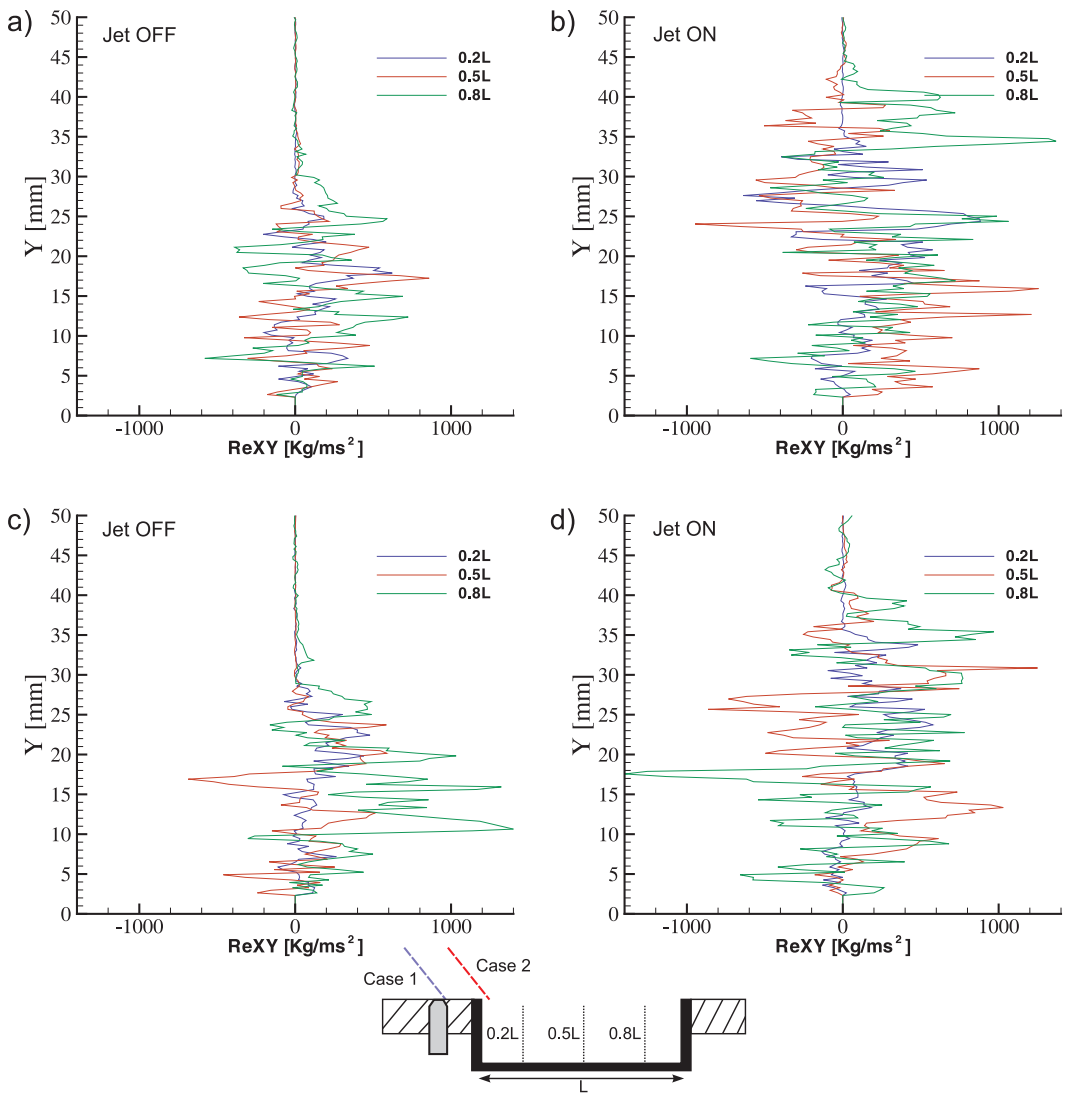

FIG. 12: Reynolds stress profiles along the cavity relating to Figure 11: (a) & (b) Case 1, (c) & (d) Case 2.

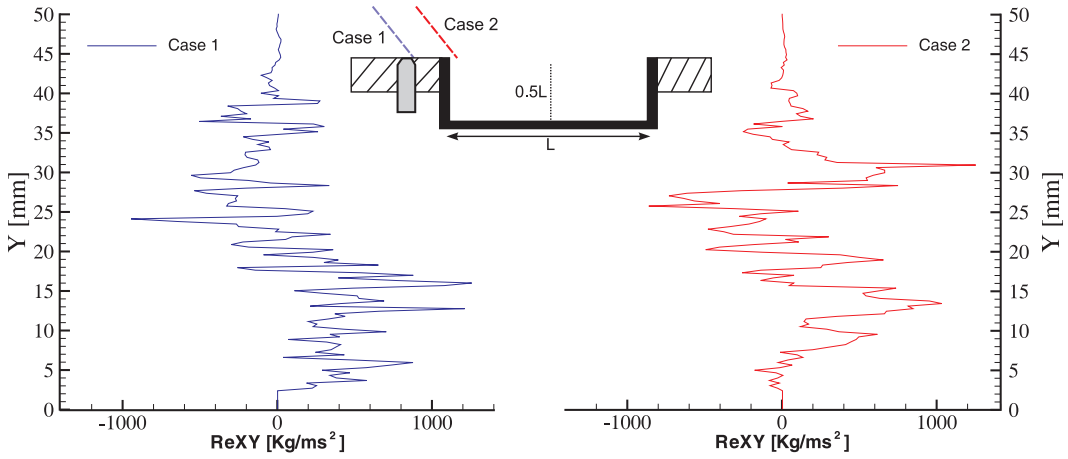

FIG. 13: Reynolds stress profiles for Case 1 and Case 2 at the cavity centreline of 0.5L.

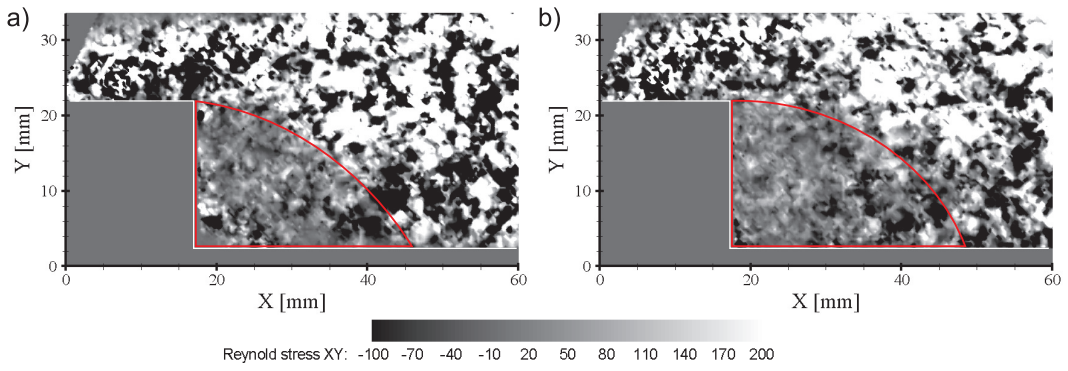

FIG. 14: Zoomed areas of Reynolds stress: (a) Case 1, (b) Case 2 (the scales have been saturated to better discern the flow near the leading edge wall).